

# High-energy sources at low radio frequency: the Murchison Widefield Array view of *Fermi* blazars

M. Giroletti<sup>1,\*</sup>, F. Massaro<sup>2</sup>, R. D'Abrusco<sup>3</sup>, R. Lico<sup>4</sup>, D. Burlon<sup>5,6</sup>, N. Hurley-Walker<sup>7</sup>, M. Johnston-Hollitt<sup>8</sup>, J. Morgan<sup>7</sup>, V. Pavlidou<sup>9</sup>, M. Bell<sup>10</sup>, G. Bernardi<sup>11</sup>, R. Bhat<sup>7</sup>, J.D. Bowman<sup>12</sup>, F. Briggs<sup>13,6</sup>, R.J. Cappallo<sup>14</sup>, B.E. Corey<sup>14</sup>, A.A. Deshpande<sup>15</sup>, A. Ewall-Rice<sup>16</sup>, D. Emrich<sup>7</sup>, B.M. Gaensler<sup>5,6,17</sup>, R. Goetze<sup>16</sup>, L.J. Greenhill<sup>18</sup>, B.J. Hazelton<sup>19</sup>, L. Hindson<sup>8</sup>, D.L. Kaplan<sup>20</sup>, J. C. Kasper<sup>21</sup>, E. Kratzenberg<sup>14</sup>, L. Feng<sup>16</sup>, D. Jacobs<sup>12</sup>, N. Kurdryavtseva<sup>7</sup>, E. Lenc<sup>5,6</sup>, C.J. Lonsdale<sup>14</sup>, M. J. Lynch<sup>7</sup>, B. McKinley<sup>22</sup>, S.R. McWhirter<sup>14</sup>, D.A. Mitchell<sup>10,6</sup>, M.F. Morales<sup>19</sup>, E. Morgan<sup>16</sup>, D. Oberoi<sup>23</sup>, A.R. Offringa<sup>24</sup>, S.M. Ord<sup>7,6</sup>, B. Pindor<sup>22</sup>, T. Prabu<sup>15</sup>, P. Procopio<sup>22</sup>, J. Riding<sup>22</sup>, A.E.E. Rogers<sup>14</sup>, A. Roshni<sup>25</sup>, N. Udaya Shankar<sup>15</sup>, K. S. Srivani<sup>15</sup>, R. Subrahmanyan<sup>15,6</sup>, S. J. Tingay<sup>7,6</sup>, M. Waterson<sup>26,7</sup>, R. B. Wayth<sup>7,6</sup>, R. L. Webster<sup>22,6</sup>, A. R. Whitney<sup>14</sup>, A. Williams<sup>7</sup>, C. L. Williams<sup>16</sup>

(Affiliations can be found after the references)

Received ; accepted

## ABSTRACT

**Context.** Low-frequency radio arrays are opening a new window for the study of the sky, both to study new phenomena and to better characterize known source classes. Being flat-spectrum sources, blazars are so far poorly studied at low radio frequencies.

**Aims.** We characterize the spectral properties of the blazar population at low radio frequency compare the radio and high-energy properties of the gamma-ray blazar population, and search for radio counterparts of unidentified gamma-ray sources.

**Methods.** We cross-correlated the 6,100 deg<sup>2</sup> Murchison Widefield Array Commissioning Survey catalogue with the Roma blazar catalogue, the third catalogue of active galactic nuclei detected by *Fermi*-LAT, and the unidentified members of the entire third catalogue of gamma-ray sources detected by *Fermi*-LAT. When available, we also added high-frequency radio data from the Australia Telescope 20 GHz catalogue.

**Results.** We find low-frequency counterparts for 186 out of 517 (36%) blazars, 79 out of 174 (45%) gamma-ray blazars, and 8 out of 73 (11%) gamma-ray blazar candidates. The mean low-frequency (120–180 MHz) blazar spectral index is  $\langle\alpha_{\text{low}}\rangle = 0.57 \pm 0.02$ : blazar spectra are flatter than the rest of the population of low-frequency sources, but are steeper than at  $\sim$ GHz frequencies. Low-frequency radio flux density and gamma-ray energy flux display a mildly significant and broadly scattered correlation. Ten unidentified gamma-ray sources have a (probably fortuitous) positional match with low radio frequency sources.

**Conclusions.** Low-frequency radio astronomy provides important information about sources with a flat radio spectrum and high energy. However, the relatively low sensitivity of the present surveys still misses a significant fraction of these objects. Upcoming deeper surveys, such as the GaLactic and Extragalactic All-Sky MWA (GLEAM) survey, will provide further insight into this population.

**Key words.** BL Lacertae objects: general, catalogues, gamma rays: galaxies, quasars: general, radiation mechanisms: non-thermal, radio continuum: galaxies

## 1. Introduction

Blazars are the most numerous source population in gamma-ray catalogues (Abdo et al. 2010; Nolan et al. 2012; Acero et al. 2015). They are radio-loud active galactic nuclei (AGNs) with relativistic jets pointing near to the line of sight. They include flat-spectrum radio quasars (FSRQ), with prominent emission lines in their optical spectra, and BL Lac objects (BL Lacs), with nearly featureless optical spectra. In addition to these markedly different emission line properties, the two classes also have other observational differences; however, the underlying physical processes at work in the two classes are the same, with a beamed relativistic jet powered by accretion onto a supermassive black hole dominating the spectral energy distribution (SED) from radio to gamma rays. In the radio band, at GHz frequencies, blazars of all classes show a flat spectrum ( $\alpha < 0.5$ , in the  $S(\nu) \propto \nu^{-\alpha}$  convention). Several recent works demonstrated that blazars largely also maintain a flat spectrum at lower frequency, down to the

300 MHz band (Massaro et al. 2013a; Nori et al. 2014) and even 74 MHz (Massaro et al. 2013b). However, these studies were based on the comparison of data from low-frequency surveys to  $\sim$  GHz surveys carried out at a different epoch. Therefore, they provide only two-point non-simultaneous spectra, which could be affected by time variability (a key feature of blazars), and they are not sensitive to any possible curvature, important information about the physical properties of the emission region, such as the relative contribution of different spectrum components, and breaks in the electron energy distribution.

In the context of the Murchison Widefield Array (MWA, Tingay et al. 2013) instrument commissioning, Hurley-Walker et al. (2014) performed the Murchison Widefield Array Commissioning Survey (MWACS). The MWACS is a multi-wavelength low-frequency radio sky survey, covering approximately 6,100 square degrees in the southern sky over three bands centred at 119, 150, and 180 MHz. Nearly at the same time, Massaro et al. (2015) published the fifth edition of the Roma-BZCat, the most recent multi-wavelength list of blazars.

\* Email: giroletti@ira.inaf.it

**Table 1.** List of quantities.

Symbol	Quantity
$S_{0.18}$	flux density at 180 MHz (from MWACS)
$S_1$	flux density at $\sim 1$ GHz (0.8 GHz from SUMSS or 1.4 GHz from NVSS, if Dec. $< -30^\circ$ or $> -30^\circ$ , respectively)
$S_{20}$	flux density at 20 GHz (from AT20G)
$\alpha_{\text{low}}$	spectral index between 120 and 180 MHz (MWACS)
$\alpha_{0.18-1}$	spectral index between 180 MHz and $\sim 1$ GHz
$\alpha_{1-20}$	spectral index between $\sim 1$ and 20 GHz

At the other end of the electromagnetic spectrum, Acero et al. (2015) have just released the third *Fermi*-LAT catalogue of gamma-ray sources (3FGL), based on Large Area Telescope (LAT) data collected with a longer exposure and an improved instrument and analysis characterization; furthermore, Ackermann et al. (2015) have realized the accompanying third catalogue of LAT active galactic nuclei (3LAC). These surveys therefore represent an invaluable resource to tackle the spectral characterization of gamma-ray blazars at low frequency with unprecedented detail and to discuss statistical significance and physical implications of the correlation between emission in the two bands. Indeed, Ackermann et al. (2011a) have studied with great accuracy the radio-gamma connection in the several GHz radio band, while only preliminary studies have been attempted for low-frequency radio data.

In this paper, we cross-correlate the MWACS catalogue with the BZCat, the 3LAC, and the list of unassociated sources of the 3FGL; when available, we also add high-frequency data from the Australia Telescope 20 GHz survey (AT20G, Murphy et al. 2010). All cross-correlations and analyses are carried out within the MWACS footprint, which is given in Sect. 2, along with an outline of the other radio and gamma-ray surveys and catalogues. Then we describe in Sect. 3 the construction of our working samples (blazars in the MWACS, gamma-ray AGNs in the MWACS, other gamma-ray sources in the MWACS) and present their overall properties in Sect. 4; finally, we discuss the results and give our conclusions in Sect. 5.

Throughout the paper, we use a  $\Lambda$ CDM cosmology with  $h = 0.71$ ,  $\Omega_m = 0.27$ , and  $\Omega_\Lambda = 0.73$  (Komatsu et al. 2009). The radio spectral index  $\alpha$  is defined such that  $S_\nu \propto \nu^{-\alpha}$  and the gamma-ray photon index  $\Gamma$  such that  $dN_{\text{photon}}/dE \propto E^{-\Gamma}$ . In Table 1 we give a list of the quantities used for flux densities and spectral indices throughout the paper.

## 2. Selected surveys and catalogues

### 2.1. MWACS catalogue

The MWACS catalogue (Hurley-Walker et al. 2014) is our main reference catalogue; we downloaded the final table from Vizier<sup>1</sup>. This catalogue lists 14,110 sources, in the sky area approximately  $0^\circ \leq \text{R.A.} \leq 127.5^\circ$  or  $307.5^\circ \leq \text{R.A.} \leq 360^\circ$  ( $20.5^{\text{h}} \leq \text{R.A.} \leq 8.5^{\text{h}}$ ) and  $-58.0^\circ < \text{Dec.} < -14.0^\circ$ . Data were taken in October 2012. All the sources in this area have high absolute Galactic latitude, which is ideal for blazar studies (e.g. the 3LAC only contains high-latitude sources by construction).

For each source, the catalogue reports the flux density  $S_{0.18}$  at 180 MHz and the spectral index  $\alpha_{\text{low}}$  derived across the three frequency bands centred on 119, 150, and 180 MHz. The survey has  $\sim 3'$  angular resolution and a typical noise level of 40 mJy

beam<sup>-1</sup>, with reduced sensitivity near the field boundaries and bright sources. The faintest source has  $S_{0.18} = 0.12$  Jy. Sources are marked with a spectral fit flag if the identification at the three frequencies is problematic: a type 1 fit classification indicates a spectral index determined by integrating an extended source, and a type 2 a forced fit.

### 2.2. BZCat

The BZCat is a multi-wavelength list of blazars, regularly updated since the release of the first edition in 2009 (Massaro et al. 2009). Massaro et al. (2015) have recently released the fifth edition, in which they report coordinates, redshift, and multi-frequency (radio, millimetre, optical, X-ray, and gamma-ray) data for 3561 sources. The sources are classified as FSRQs, BL Lacs, and BL Lacs with significant contamination from the host galaxy, or blazars of uncertain type (BCU). All the sources in the BZCat are detected in the radio, and we used the radio flux density at  $\sim 1$  GHz as reported in the catalogue: the radio data reported in the BZCat come partly from the NRAO VLA Sky Survey (NVSS, Condon et al. 1998) at 1.4 GHz or the Sydney University Molonglo Sky Survey (SUMSS, Bock et al. 1999; Mauch et al. 2003) at 0.8 GHz, for sources above or below Dec. =  $-30^\circ$ , respectively. In the following, we simply indicate this radio flux density as  $S_1$ ; however, we considered the actual frequency at which the flux density was obtained whenever we used it to determine the spectral index.

### 2.3. 3FGL

The third *Fermi*-LAT catalogue (3FGL) is the deepest in the 100 MeV–300 GeV energy range. It is based on the first four years of science operation data from the *Fermi* mission, between 2008 August 4 and 2012 July 31, and it includes 3033 sources. Each source is characterized by its position, gamma-ray flux (photon flux, energy flux, flux in different energy ranges and in 48 monthly time bins), and photon index. The typical 95% positional confidence radius is  $\sim 0.1^\circ$ . Most 3FGL sources are identified with or statistically associated with<sup>2</sup> blazars (see Sect. 2.4), but about one-third of the 3FGL does not have a plausible counterpart at other wavelengths. These so-called unassociated gamma-ray sources (hereafter, UGS) are not distributed uniformly in the sky: 468 fall in the Galactic plane ( $|b| < 5^\circ$ ); they are most likely a mix of galactic and extragalactic discrete sources embedded in complex diffuse emission; the remaining 542 sources are presumably of extragalactic nature, possibly faint and as yet unrecognised blazars. In the present work, we have considered the data available through the *Fermi* Science Support Center<sup>3</sup>.

### 2.4. 3LAC

The third LAT AGN catalogue (3LAC) includes a total of 1563 gamma-ray sources among the 2192  $|b| > 10^\circ$  3FGL sources. These 3LAC sources are identified or statistically associated with AGNs by means of a Bayesian association (Abdo et al. 2010) or a likelihood ratio (Ackermann et al. 2011b) method. These 1563 gamma-ray sources are associated with 1591 objects

<sup>2</sup> An identification is claimed when correlated variability is observed, while the more common association between LAT sources and AGNs is based on statistical methods.

<sup>3</sup> [http://fermi.gsfc.nasa.gov/ssc/data/access/lat/4yr\\_catalog/gll\\_psc\\_v16.fit](http://fermi.gsfc.nasa.gov/ssc/data/access/lat/4yr_catalog/gll_psc_v16.fit)

<sup>1</sup> <ftp://cdsarc.u-strasbg.fr/pub/cats/VIII/98>

**Table 2.** Low-frequency detection rates for BZCat and 3LAC source classes in the MWACS footprint.

Class	BZCat		3LAC	
	ratio	%	ratio	%
Total	186/517	36%	87/247	35%
FSRQ	147/327	45%	52/71	73%
BLL	23/153	15%	19/87	22%
BCU	16/37	43%	8/16	50%
Candidates	...	...	8/73	11%

**Notes.** By construction, the BZCat does not contain blazar candidates. For the 3LAC, we did not include radio galaxies.

(28 sources have double associations), consisting mostly (98%) of blazars or blazar candidates.

From the entire sample, Ackermann et al. (2015) have defined a “clean” subset of 3LAC single-association sources free of any analysis problems (e.g. sources strongly affected by changes in the diffuse emission model). In the following, whenever we mention the 3LAC we implicitly refer to this clean subset, which includes 1444 objects with 414 FSRQs, 604 BL Lacs, 49 BCUs, 353 blazar candidates, and 24 non-blazar AGNs.

We note that Ackermann et al. (2015) classify as blazar candidates both confirmed blazars of uncertain type (which have an optical spectrum and are also included in BZCat) and other blazar candidates (which do not appear in BZCat, but still present multi-wavelength features typical of blazars, such as a flat radio spectrum or a two-humped broadband SED). For consistency with the BZCat, we here consider separately gamma-ray blazars of uncertain type (which we indicate as BCU, as in BZCat) and gamma-ray blazar candidates.

In particular, we carried out our analysis starting from the machine-readable form of Table 4 in Ackermann et al. (2015)<sup>4</sup>.

### 2.5. AT20G

The Australia Telescope 20 GHz (AT20G) survey is a radio survey carried out at 20 GHz with the Australia Telescope Compact Array (ATCA). It covers the whole sky south of Dec.  $< 0^\circ$  and includes 5890 sources above a 20 GHz flux-density limit of 40 mJy. The survey was carried out in two steps from 2004 to 2008: in a first phase, the ATCA realized a fast-scanning blind survey characterized by an overall rms noise of  $1\sigma \sim 10$  mJy beam<sup>-1</sup>; then, all the sources brighter than 50 mJy were followed up to produce the final catalogue, with additional near-simultaneous flux-density measurements at 5 and 8 GHz for most sources.

The source composition of the AT20G is rather heterogeneous; however, high-frequency observations naturally favour the detection of flat-spectrum sources like blazars and in particular gamma-ray blazars (Mahony et al. 2010). As it also covers the entire MWACS footprint, we used it to complement the MWA data with higher frequency information for the blazar samples that we describe in the following section. In particular, we made use of the data in version 1.0 provided by the Vizier archive<sup>5</sup>.

## 3. Sample construction

After restricting the BZCat, the 3LAC, and the 3FGL lists to the MWACS footprint, we cross-matched them with the MWACS

catalogue using TOPCAT (Taylor 2005). In the following subsections, we give details of the procedure.

### 3.1. BZCat-MWACS sample

Within the entire MWACS field, the BZCat contains 517 sources, divided into 153 BL Lacs, 327 FSRQs, and 37 blazars of uncertain kind. We cross-matched this subset with the MWACS catalogue, using a positional uncertainty of  $5''$  on the BZCat coordinates and the  $95\%$  confidence error ellipse for each MWACS source (obtained as  $1.621 \times$  the R.A. and Dec.  $1\sigma$  uncertainty reported in the MWACS catalogue). The  $5''$  value for the BZCat positions is very conservative for most sources, some of which have positions from VLBI observations that are accurate at the subarcsecond level. However, we verified that a few additional sources are picked up if we increase the uncertainty from  $1''$  to  $5''$ , although further increases do not pick up any more sources.

We also tried to cross-match the two catalogues with a fixed radius, using the same procedure based on the generation of 100 mock replicas that we adopted in our previous papers (Massaro et al. 2013a,b, 2014). This method provided a sanity check that the errors quoted in the MWACS catalogue are sensible. Therefore, we continued our analysis using the rigorous association method based on the source-by-source uncertainty. The accuracy of the MWA coordinates is affected by two components, one of random intensity that is due to the ionospheric phase contribution, and one dependent on the source flux density. Since sources with higher flux density have better constrained positions, this method maximizes the efficiency of our selection and the use of information retained from the data.

In total, we found 186 matches: 23 BL Lacs, 147 FSRQs, and 16 blazars of uncertain type. Within these 186 matches, 10 sources have MWACS spectral fit classification of type 1 or 2 (five sources of each type). By constructing 100 mock replicas of the BZCat sample, in which we shifted each position by  $2^\circ$  along a random position angle, and repeating the association procedure for each replica, we estimate that less than 1 of these 186 matches arises by chance (on average, 0.8 sources per fake sky).

We furthermore collected high-frequency data for the BZCat-MWACS sample by cross-correlating it with the AT20G survey catalogue. Murphy et al. (2010) calculated the uncertainty in right ascension and declination for the full AT20G sample as  $\sigma_{\text{RA}} = 0.9''$  and  $\sigma_{\text{Dec}} = 1.0''$ , respectively. Using these values for AT20G and extending the positional uncertainty for BZCat sources from  $1''$  to  $5''$ , the number of matches increases from 155 to 170, and then does not increase any further up to  $30''$ . We then considered all the 170 matches as bona fide associations. The 16 sources that do not have a match are all rather faint at both 180 MHz and 1 GHz, and they also have a steep spectral index ( $\langle \alpha_{0.18-1} \rangle = 0.68$ ) and extrapolated flux densities generally below the AT20G sensitivity.

### 3.2. 3LAC-MWACS sample

The subset of the clean 3LAC sources localized within the MWACS footprint contains 249 objects; there are 87 BL Lacs, 71 FSRQ, 16 BCU, 73 blazar candidates, and 2 radio galaxies.

Similar to the BZCat sources, these objects have accurately known coordinates, therefore we followed the same association method described above. We stress that we used the positions of the low-energy counterparts listed in the 3LAC and not those of the gamma-ray sources, which are significantly less well deter-

<sup>4</sup> [http://iopscience.iop.org/0004-637X/810/1/14/suppdata/apj517471t4\\_mrt.txt](http://iopscience.iop.org/0004-637X/810/1/14/suppdata/apj517471t4_mrt.txt)

<sup>5</sup> <ftp://cdsarc.u-strasbg.fr/pub/cats/J/MNRAS/402/2403>

mined and could result in a large number of spurious associations.

From our starting list, we found counterparts in the MWACS for 88 3LAC sources, divided into 19 BL Lacs, 52 FSRQ, 8 BCU, 8 blazar candidates, and 1 radio galaxy (PKS 0625–35). We note that the other LAT radio galaxy (Pictor A) does indeed appear in the MWACS data as a bright source, but was not entered in the final MWACS catalogue because of calibration difficulties brought about by its high brightness and large extent. It therefore does not enter our catalogue cross-correlation either. Given the very low statistics for the population of gamma-ray radio galaxies, in the following we only focus on the 87 3LAC blazars and blazar candidates with counterparts in the MWACS. All but three of the sources (PKS 0451–28, PKS 2245–328, and PKS 2333–415) have spectral fit class 0. Following the same procedure as in Sect. 3.1 and considering the smaller number of sources in this case, we do not expect more than one of these matches to be spurious.

We also cross-matched this sample of 87 sources with the AT20G catalogue and obtained 81 matches. The six missing sources again have fairly steep spectral indices ( $\langle\alpha_{0.18-1}\rangle = 0.66$ ) and low extrapolated flux densities (only the blazar candidate PKS 0302–16 exceeds an extrapolated flux density of  $S_{20} = 100$  mJy).

### 3.3. Other gamma-ray sources in the MWACS

The MWACS footprint covers 96 3FGL UGS. These sources have by definition no clearly localized counterpart, therefore we performed the cross correlation of this list with MWACS catalogue using the 95% confidence radius for each gamma-ray source that is reported in the 3FGL and the positional uncertainty associated with the MWACS coordinates as described in Sect. 3.1. We found 13 MWACS counterparts for 10 UGS, with seven single matches and three double matches. Three sources have a spectral index flag of 1, and one has 2.

Given the large positional uncertainty of the UGS positions and the local space density of the MWACS sources, we investigated the possibility that these are chance matches. To do this, we created 100 mock replicas of the UGS list, shifting the position by  $2^\circ$  in a random position angle, and repeated the association procedure with the same method as in the original list. We find  $15 \pm 3$  MWA matches even starting with a random UGS catalogue.

For completeness, we also cross-correlated the remaining sources in the 3FGL (i.e. those that are neither associated with AGNs nor are UGS), again using the gamma-ray positional uncertainty. We found three more matches: two pulsars (PSR J0437–4715, PSR J0742–2822) and one starburst galaxy (NGC 253).

## 4. Results

Our three catalogues are presented in Tables 5–7, that are the list of MWACS sources associated with BZCat blazars (Table 5), with 3LAC gamma-ray blazars (Table 6), and with un-associated 3FGL gamma-ray sources (Table 7). In the next three subsections, we analyse these catalogues.

### 4.1. Blazars in the MWACS: catalogue and demographics

The 186 matches between BZCat and MWACS listed in Table 5 correspond to a detection rate of 36%. In Cols. 2 and 3 of Table

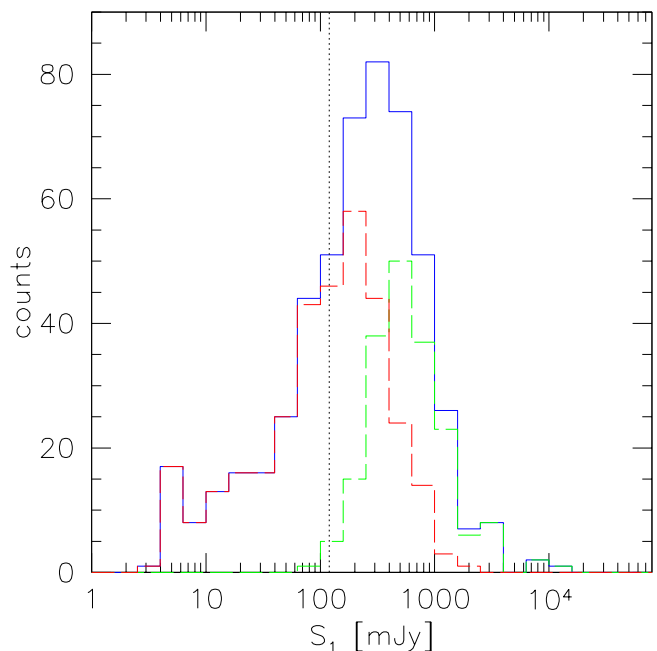


**Fig. 1.** Blazar flux density distribution at 1 GHz for the entire BZCat (blue solid line) and for the detected (green dashed line) and not detected (red dashed line) subset in MWACS. The dotted vertical line corresponds to  $S_1 = 120$  mJy, i.e. the flux density limit of the MWACS survey extrapolated with  $\alpha = 0.0$ .

2, we report the detection rates divided by source class, which is clearly higher for FSRQs (45%) than for BL Lacs (15%); BCUs appear to have a similar detection rate as FSRQs (albeit with some uncertainty due to the small sample size).

In Fig. 1 we plot the histogram of the  $\sim 1$  GHz flux density for the entire BZCat sources divided into two subsets according to whether they were detected at low frequency (green histogram) or not (red histogram). This plot shows that the MWACS detection probability has a strong dependence on the GHz flux density; in other words, the faintest blazars are very rarely associated with MWACS counterparts. This immediately explains the highest detection rate found for FSRQs, since FSRQs are on average brighter than BL Lacs. However, it is still remarkable that about a half of the not detected blazars still have a  $\sim 1$  GHz flux density higher than that of the faintest source in the MWACS catalogue (167/331 sources have  $S_1 > 120$  mJy). If these sources had non-inverted spectra ( $\alpha_{0.18-1} \geq 0.0$ ), we would expect them to be detected by MWACS, which implies that they have either an inverted spectrum or that they are strongly variable.

In Fig. 2 we also plot the simultaneous low-frequency spectral index  $\alpha_{\text{low}}$  distribution for the entire MWACS catalogue and for the blazars. The cumulative distribution is also shown in the right panel. Even in the 120–180 MHz range, blazars have much flatter spectra than the rest of the radio sources in the extragalactic sky: the weighted average MWACS spectral index for blazars is  $\langle\alpha_{\text{low}}\rangle = 0.57 \pm 0.02$ , significantly flatter than the one obtained for the entire MWACS population, for which it is  $\langle\alpha_{\text{low}}\rangle = 0.866 \pm 0.002$ . FSRQs are marginally steeper ( $\langle\alpha_{\text{low}}\rangle = 0.56 \pm 0.02$ ) than BL Lacs ( $\langle\alpha_{\text{low}}\rangle = 0.49 \pm 0.05$ ).

For each source, we also calculated the non-simultaneous spectral index  $\alpha_{0.18-1}$  between 180 MHz and  $\sim 1$  GHz. The results show a flattening of the spectra from low to higher frequency for FSRQs of about  $\langle\Delta\alpha\rangle = \langle\alpha_{0.18-1}\rangle - \langle\alpha_{\text{low}}\rangle \sim -0.25$ , while BL Lacs maintain the same spectral index. This difference

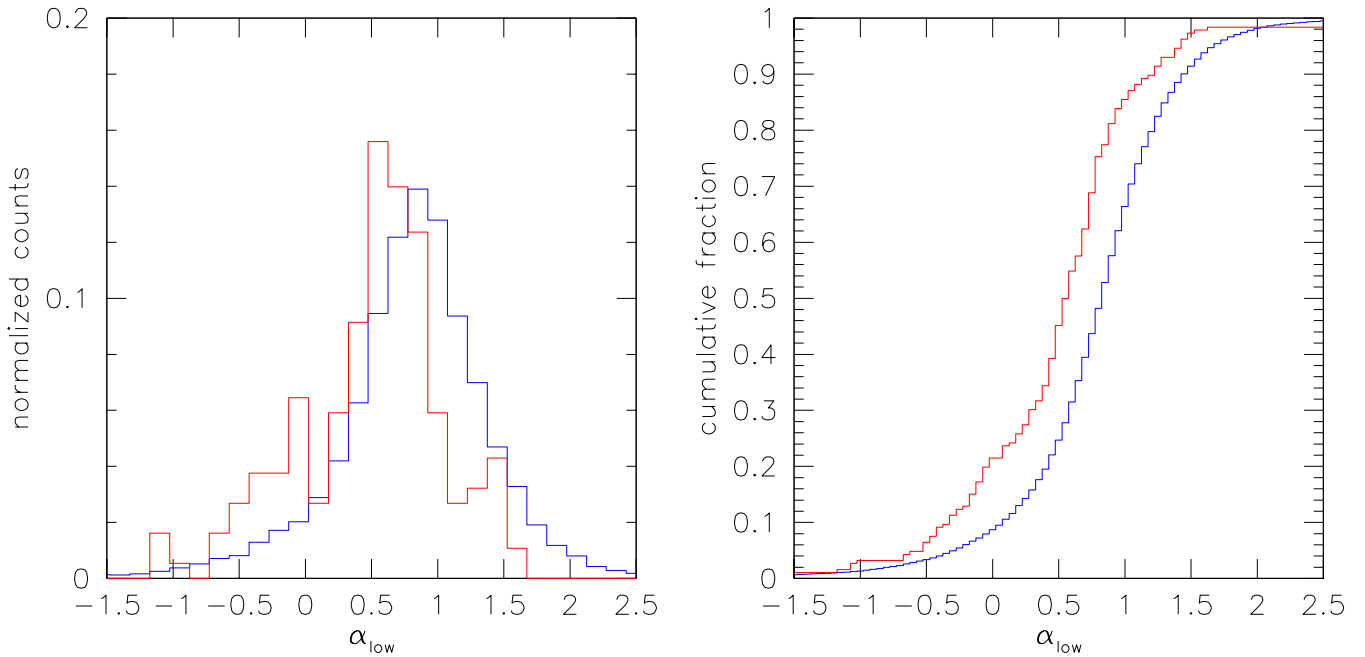


**Fig. 2.** Low-frequency spectral index counts (left) and cumulative (right) distributions for the entire MWACS catalogue (blue line) compared with BZCat-MWACS blazars (red line). Because the population counts are very different, normalized distributions are shown. The  $x$ -axis range is limited to the interval  $-1.5 < \alpha_{\text{low}} < 2.5$  for illustration purposes.

**Table 3.** Average spectral indices for BZCat and 3LAC source classes.

Sample (1)	Class (2)	$\langle \alpha_{\text{low}} \rangle \pm \sigma_{\langle \alpha_{\text{low}} \rangle}$ (3)	$\langle \alpha_{0.18-1} \rangle \pm \sigma_{\langle \alpha_{0.18-1} \rangle}$ (4)	$n_{\text{low}, 0.18-1}$ (5)	$\langle \alpha_{1-20} \rangle \pm \sigma_{\langle \alpha_{1-20} \rangle}$	$n_{1-20}$
BZCat-MWACS	Total	$0.57 \pm 0.02$	$0.337 \pm 0.013$	186	$0.096 \pm 0.004$	170
	FSRQ	$0.56 \pm 0.02$	$0.297 \pm 0.014$	147	$0.097 \pm 0.005$	139
	BLL	$0.49 \pm 0.05$	$0.46 \pm 0.03$	23	$0.105 \pm 0.014$	18
3LAC-MWACS	Total	$0.50 \pm 0.03$	$0.305 \pm 0.017$	87	$0.074 \pm 0.005$	81
	FSRQ	$0.49 \pm 0.04$	$0.18 \pm 0.02$	52	$0.038 \pm 0.006$	52
	BLL	$0.42 \pm 0.06$	$0.39 \pm 0.04$	19	$0.138 \pm 0.012$	17

**Notes.** For each set, we report the weighted average and the error on the weighted average. Weights  $w_i$  on each spectral index  $\alpha_i$  are determined as  $1/\sigma_i$ , where  $\sigma_i$  is the uncertainty on the spectral index as provided in the MWACS catalogue at low frequency, or is determined through propagation of the uncertainty on the measured flux density for  $\alpha_{0.18-1}$  and  $\alpha_{1-20}$ . The weighted average is then  $\langle \alpha \rangle = \sum_{i=1}^n w_i \alpha_i / \sum_{i=1}^n w_i$  and the associated error is  $\sigma_{\langle \alpha \rangle}^2 = 1 / \sum_{i=1}^n w_i$ .

between FSRQs and BL Lacs stems from the average low flux density of BL Lacs at  $\sim 1$  GHz because faint sources can reach the MWACS detection threshold more easily if they steepen at low frequency.

Finally, for the subset of sources with AT20G counterparts, we also computed the high-frequency spectral index  $\langle \alpha_{1-20} \rangle$  between  $\sim 1$  and 20 GHz. In this frequency range, the spectra are much flatter ( $\langle \alpha_{1-20} \rangle = 0.096 \pm 0.004$ ), and no difference is found between FSRQs and BL Lacs. We report all the weighted mean values and the associated errors for the spectral indices in the various frequency ranges in Table 3.

#### 4.2. Gamma-ray blazars in the MWACS: catalogue and demographics

Table 6 reports the list of the 87 matches between the 3LAC and the MWACS catalogues. In Table 2 (Cols. 4 and 5) we also report the detection rate for the entire sample and for the individual sub-classes. The overall low-frequency detection rate is 35.2%. If we only consider the confirmed blazars, however, it increases

to 45.4%, which is significantly higher than for the overall blazar population discussed in Sect. 4.1. In the sub-classes, the detection rate is highest for FSRQ (73.2%) and much lower for BL Lacs (21.8%); BCUs are in between (50.0%). Again, within each single class, gamma-ray detected sources have a larger detection rate at low frequency than the same kind of sources considered independently of their gamma-ray activity. Blazar candidates have a low detection rate of 11.0%, not surprisingly given their low average 1 GHz radio flux densities.

In Fig. 3 we show the histogram of the gamma-ray energy flux above  $E > 100$  MeV averaged over the four years of the *Fermi*-LAT data. We indicate separately the set of all the 3LAC sources and the subsets of MWACS detected and not detected sources. The detected sources have higher gamma-ray fluxes or, in other words, the MWACS detection rate is higher for higher gamma-ray fluxes. Moreover, the detection rate above  $4 \times 10^{-11}$  erg cm $^{-2}$  s $^{-1}$  is 76% (16/21) and quite uniform across source types. The lower overall MWACS detection rate for BL Lacs with respect to FSRQs arises from the lower gamma-ray

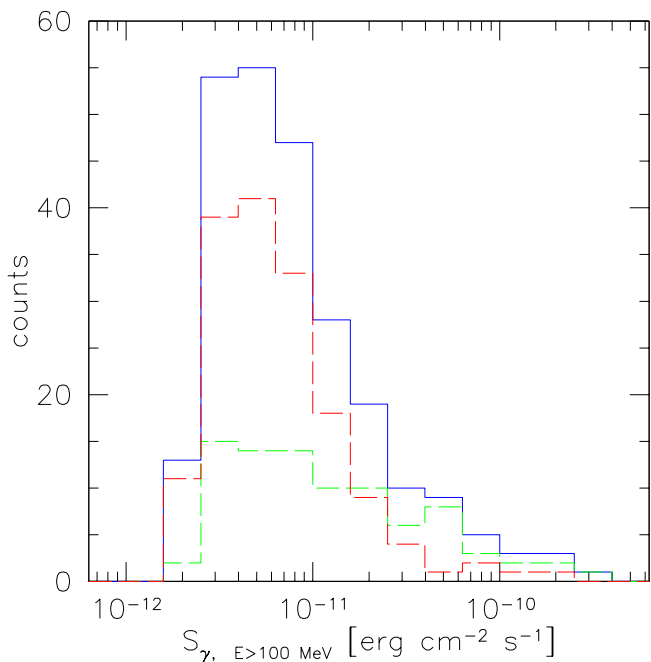


**Fig. 3.** Gamma-ray flux at  $E > 100$  MeV distribution for the entire 3LAC sample (solid blue line). Dashed lines show separately the distribution for 3LAC sources with or without an MWACS counterpart (green and red lines, respectively).

flux sources. This indicates that long-term gamma-ray and low-frequency radio fluxes are somehow correlated (see Sect. 4.3).

The low-frequency spectral index of the gamma-ray blazars is slightly flatter (by about  $\Delta\alpha = 0.07$ ) than the index of the entire blazar population (Table 3, Col. 3). Some flattening is also present in the low-to-mid and mid-to-high spectral indices. For the whole gamma-ray population and within each sub-class, the trend overall is one of flatter spectral indices as higher frequency ranges are considered.

#### 4.3. Radio and gamma-ray correlation

As suggested in the previous section, it is relevant to search for a possible correlation between low-frequency radio flux densities and gamma-ray fluxes in blazars. We show in Fig. 4 the scatter plot of the gamma ray energy flux at  $E > 100$  MeV vs.  $S_{0.18}$ . The  $x$ -axis range starts at  $S_{0.18} = 120$  mJy, which corresponds to the lowest flux density of sources included in the MWACS. Below this threshold, we show the distribution of the gamma-ray flux for the blazars not detected in MWACS.

A simple linear fit yields a slope of  $m = 0.32 \pm 0.13$ , a linear correlation coefficient of  $r = 0.26$ , and a null-hypothesis  $p$ -value of  $p = 1.5 \times 10^{-2}$ , with 87 data points. This fit is somewhat influenced by the brightest radio source (PKS 0521–36). When we exclude this source from the sample, however, we still obtain a correlation coefficient of  $r = 0.22$  and a slightly flatter, but still consistent, slope  $m = 0.30 \pm 0.14$ . To assess the significance of the observed correlation for the detected sources, we carried out a dedicated analysis based on the method described by Pavlidou et al. (2012) that has been applied by Ackermann et al. (2011a); this method combines data randomization in luminosity space (to ensure that the randomized data are intrinsically, and not just apparently, uncorrelated) and significance assessment in flux space (to explicitly avoid Malmquist bias and automatically ac-

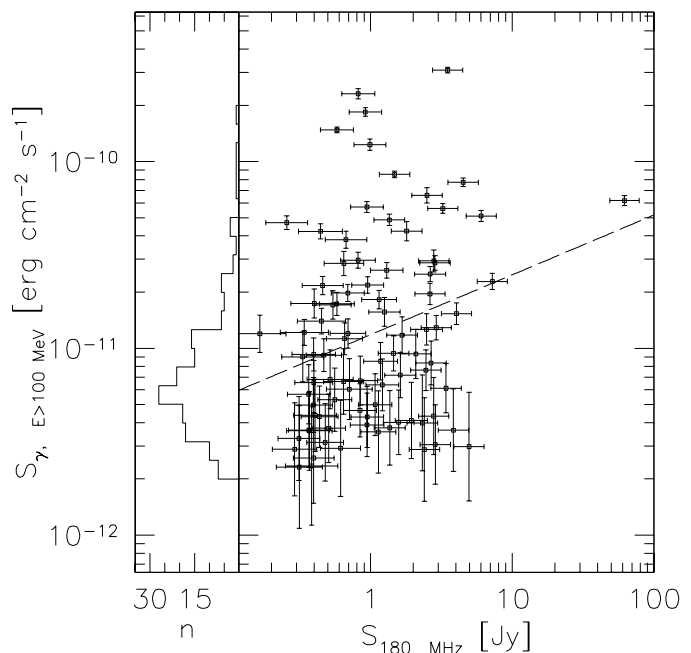


**Fig. 4.** *Fermi*-LAT gamma-ray and MWACS fluxes for 3LAC blazars. In the main panel (right), we show the 4 yr gamma-ray energy flux at  $E > 100$  MeV vs. MWACS radio flux density at 180 MHz; the dashed line is the best-fit linear regression. In the smaller left panel, we show the gamma-ray flux distribution for blazars that are not detected in MWACS; gamma-ray flux increases along the  $y$ -axis, and simple counts increase right-to-left along the  $x$ -axis.

count for the limited dynamic range in both frequencies and the presence of undetected sources). Since the method randomizes luminosities, we considered only sources with a measured redshift, which constitute the large majority of our sample (76 out of 87); moreover, it was shown that for reasonable assumptions on the redshift distribution of the sources without a known  $z$ , the method provides a conservative estimate of the significance.

We show the results in Table 4. The observed distributions provide evidence of only a low-significance correlation for the entire population ( $p = 6.1 \times 10^{-2}$ ), and of no significant correlation at all when only FSRQs are considered ( $p = 0.15$ ). We did not consider other smaller sub-samples (e.g. only BL Lacs, or only the flattest spectrum sources) because the number of objects would not have provided a statistically significant result.

The histogram in the left panel of Fig. 4 shows that the gamma-ray flux distribution of the gamma-ray blazars without a MWACS counterpart is consistent with the trend estimated for the detected sources. Future, deeper low-frequency surveys will probe this population and provide deeper insight into the possible correlation.

#### 4.4. Other gamma-ray sources in the MWACS

We list in Table 7 the ten UGS that have one or more counterparts in the MWACS catalogue. Given the high spatial density of MWACS sources, it is not possible to claim any of them as a statistically significant association. We nonetheless list them here as a reference for possible follow-ups. In particular, 3FGL J0026.2–4812 and 3FGL J2130.4–4237 are spatially consistent with two moderately bright and flat-spectrum MWACS and SUMSS sources: MWACS J0025.6–4816, with

**Table 4.** Correlation coefficient and significance for gamma-ray vs. MWACS data.

Sample (1)	# objects (2)	# redshift bins (3)	$r$ (4)	$\rho$ (5)	$p$ -value (6)
All sources	87	–	0.26	0.27	–
All sources, with $z$	76	7	0.29	0.31	$6.1 \times 10^{-2}$
FSRQ	52	5	0.21	0.25	0.15

**Notes.** In each row, we indicate the sample considered in Col. (1), the number of objects included (Col. 2), and the redshift bins used for the statistical analysis (Col. 3), the Pearson  $r$  and Spearman  $\rho$  correlation coefficients and the statistical significance for the correlation between MWACS flux density and gamma-ray energy flux  $S_\gamma$  (Cols. 4, 5, and 6) determined using the method of Pavlidou et al. (2012). The method does not consider sources without a measured redshift, therefore values in Cols. 3 and 6 are not determined for the entire sample.

$S_{0.18} = 0.65$  Jy and  $\alpha_{0.18-1} = 0.50$ , and MWACS J2131.1-4234, with  $S_{0.18} = 1.04$  Jy and  $\alpha_{0.18-1} = 0.63$ .

## 5. Discussion and conclusions

The MWACS is at present the deepest wide-area survey at low frequency. By comparison, the VLA Low-frequency Sky Survey (VLSS Cohen et al. 2007) has a typical rms noise level of  $\langle \sigma \rangle \approx 0.1$  Jy beam $^{-1}$ . The VLSS blazar detection rate reported by Massaro et al. (2013b) was only  $\sim 26\%$ , so that the sample presented in Table 5 becomes the deepest low-frequency blazar sample ever assembled. Moreover, this sample has simultaneous spectral information by construction, which is extremely valuable for studying core-dominated sources like blazars.

In the widely accepted unified scheme of radio-loud AGNs (Urry & Padovani 1995), blazars are the aligned counterparts of radio galaxies; in particular, BL Lacs are the aligned counterparts of low-power, edge-dimmed FR1 radio galaxies, and FSRQs are the aligned versions of high radio power, edge-brightened FR2 radio galaxies. This scheme has met with success, and Doppler boosting of radiation emitted from relativistic jets closely aligned to our line of sight (within  $\sim 5^\circ$ ) successfully explains most observational properties of blazars. However, Doppler boosting itself makes the blazar flat-spectrum cores apparently much brighter than the extended radio lobes, which then become very hard to study unless high-sensitivity images with high angular resolution are taken. For this reason, the opening of the low radio frequency window is of great value to the study of the extended emission in blazars (Massaro et al. 2013a,b, 2014; Nori et al. 2014; Trüstedt et al. 2014), and ultimately for the full validation of the unified schemes.

Our work has shown that the MWACS spectra of the blazars in our catalogues are on average (1) flatter (by about  $\Delta\alpha \sim 0.3$ ) than those of the entire MWACS population and (2) steeper (by about  $\Delta\alpha \sim -0.2$ ) than those of the same blazar population when considered between 180 MHz and  $\sim 1$  GHz. The first fact shows that the core component still contributes significantly to the total emission. The second result is direct proof that extended, steep spectrum emission is also present in blazars.

The (mildly) significant correlation between the low-frequency flux density and the gamma-ray energy flux, which is produced in the vicinity of the jet base, is also consistent with this scenario. Various works considering higher frequency radio observations have revealed a stronger and more significant correlation between the GHz-domain and gamma-ray data, for instance for the 1LAC samples (Ackermann et al. 2011a; Mahony et al. 2010; Ghirlanda et al. 2010, 2011). The fact that the MWACS data still provide a correlation, but weaker, agrees with additional, but not overwhelming, extended emission that is not beamed and therefore not correlated with the gamma rays.

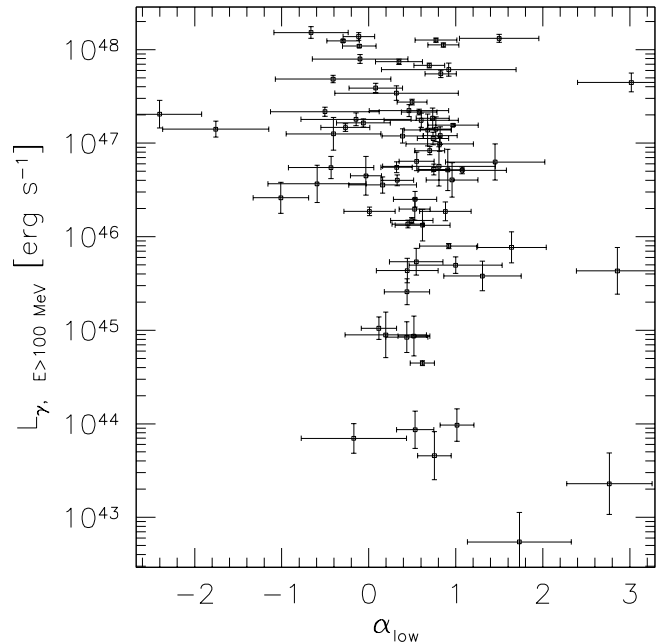


**Fig. 5.** Gamma-ray luminosity vs. low-frequency spectral index for the 3LAC-MWACS sample.

Our spectral index measurements allowed us to estimate the intensity ratio between the emission from the flat-spectrum core and the steep-spectrum lobes. We assumed that the mean spectral index of the MWACS catalogue describes the extended emission component and that the  $\alpha_{1-20}$  measured for our blazar population is a good approximation of the flat spectrum core spectral index. We decomposed the total flux density  $S(\nu)$  as

$$S(\nu) = k_c \nu^{-\alpha_c} + k_l \nu^{-\alpha_l},$$

where  $k_c$  and  $\alpha_c$  indicate the normalization and spectral index of the core component, and  $k_l$  and  $\alpha_l$  are the same quantities for the lobes. By substituting  $\alpha_c = 0.096$  and  $\alpha_l = 0.866$  and requiring that the average index between 120 and 180 MHz is  $\alpha_{\text{low}} = 0.57$ , we determined that  $k_l/k_c \sim 75$ .

Although  $k_l$  and  $k_c$ , as well as their simple ratio, have little physical meaning by themselves, they are useful since they allow us to estimate the core-to-lobe flux density ratio at any frequency. For instance, the core-to-lobe flux density ratio is  $\sim 0.53$  at 120 MHz and  $\sim 0.73$  at 180 MHz, indicating that the core still contributes at low frequency, but the majority of the flux density is emitted in the lobes. With increasing frequency, the core becomes the dominant component, with  $S_c/S_l \sim 3.5$  at 1 GHz, and as large as  $\sim 27$  at 20 GHz.

Clearly, these values are based on the mean indices and therefore are only suggestive of the average behaviour of the population. Moreover, the MWACS detected sources only constitute about 36% of the blazar population; about one half of the remaining blazars certainly have flat or inverted spectra, while we can say little about the other half. In general, these results will need to be complemented with deeper low-frequency surveys. Each single source can have wildly different contributions; in particular, the amount of Doppler beaming at the base of the jet can dramatically change the core flux and, accordingly, the component ratio. This is certainly the case for the sources with the flattest (or even inverted) MWACS spectral indices. We can directly test this by comparing the gamma-ray luminosity  $L_\gamma$  (which is affected by Doppler beaming) to  $\alpha_{\text{low}}$ . In Fig. 5 we show the plot of these two quantities. While the points are scattered, the plot shows that the most inverted sources have generally a high gamma-ray luminosity (above  $10^{46}$  erg s $^{-1}$ ), whereas the steeper sources span the entire range in luminosity, down to  $5.4 \times 10^{42}$  erg s $^{-1}$ . Of course, the situation is also complicated by several other factors, such as luminosity distance and source type.

A larger luminosity distance corresponds to higher redshift so that the observed radiation is emitted at higher frequency in the rest frame, where the spectra are flatter; this has a qualitatively similar behaviour to the one produced by the core dominance: more luminous sources have flatter spectra both because they are more beamed and because their rest-frame spectra are intrinsically flatter. In this context, we have noted in Sect. 3.1 that most sources in the BZCat-MWACS sample also have a high radio frequency counterpart in AT20G. Of the few that do not, most are typically below the AT20G sensitivity if we extrapolate from low-frequency flux density and  $\alpha_{0.18-1}$ . Interestingly, there are just two sources that have an extrapolated 20 GHz flux density higher than 100 mJy and they are both FSRQs at high redshift: 5BZQJ2300-2644 ( $z = 1.476$ ) and 5BZQJ2327-1447 ( $z = 2.465$ ), while the mean  $z$  in this sub-sample is  $z = 0.9$  (in particular, they are the second and fourth most distant in the 16 source subsample). This could suggest that the rest-frame spectrum of blazars shows a rather complex behaviour, with a new steepening at even higher frequency ( $> 20$  GHz) after the flattening between the MWA band and the few GHz domain. A similar high-frequency spectral behaviour for compact sources has been reported by Chhetri et al. (2012) and Massardi et al. (2016).

We note that the gamma-ray luminosity is generally dependent on the source type (Ackermann et al. 2011b, 2015), with FSRQs more luminous than BL Lacs. By the peak of the synchrotron component of their SED, blazars are further classified into low-, intermediate-, or high-synchrotron peaked (LSP, ISP, HSP, respectively) sources that are characterized by a synchrotron peak frequency  $\nu_{\text{peak}}$  (Hz) such that  $\log \nu_{\text{peak}} < 14$ ,  $14 < \log \nu_{\text{peak}} < 15$ , and  $\log \nu_{\text{peak}} > 15$ , respectively. The gamma-ray luminosity decreases from LSP to HSP blazars, similar to what has already been suggested for the blazar sequence by Fossati et al. (1998). While this scenario is the subject of a lively and long-lasting debate (e.g. Giommi & Padovani 2015; Potter & Cotter 2013; Meyer et al. 2011), we note that our sample is mainly composed of FSRQ (which are typically LSP blazars). The reason for this composition lies in the still somewhat limited sensitivity of the MWACS. As we have noted, the present sample is the deepest available at present; however, faint sources like BL Lacs, and HSP blazars in particular, have lower flux density, and deeper catalogues are necessary to study the blazar population in greater depth.

In the very near future, significant resources are expected to become available, such as the recently released LOw Frequency Array (LOFAR) Multifrequency Snapshot Sky Survey (MSSS, e.g. Heald et al. 2015) and the GaLactic and Extragalactic All-Sky MWA Survey (GLEAM, Wayth et al. 2015). On the path towards the Square Kilometer Array, it will be possible to greatly extend the current picture of the connection between high-energy and radio emission in blazars (Giroletti et al. 2015) and more generally between the core and extended emission in radio-loud AGNs. The new catalogues will indeed allow us to characterize the low-frequency spectral properties of the still significant population of blazars that are missed in the present work. MSSS and GLEAM, which also partly overlap, will provide a combined dataset that is ideal for studying the low-frequency properties of *Fermi*-LAT blazars (1) simultaneously and (2) for the full sky. Moreover, because the new surveys will also cover the Galactic plane, important results might be obtained in the study of pulsars and other astrophysical accelerators such as supernovae.

For UGS sources, the situation is more complicated. The spatial density of low-frequency sources is already too high to claim associations only based on the spatial coincidence, and this is bound to increase at lower flux density limits. It will be necessary to take additional features into account to recognize sources of known gamma-ray emitters. This includes for example a flat spectrum (for core-dominated blazars) or pulsed emission.

*Acknowledgements.* MG acknowledges financial support and kind hospitality during his visits at Curtin University and Sydney Institute for Astrophysics. We acknowledge financial contribution from grant PRIN-INAF-2011. This research has made use of the Vizier catalogue access tool, CDS, Strasbourg, France, and of NASA's Astrophysics Data System.

This scientific work makes use of the Murchison Radio-astronomy Observatory, operated by CSIRO. We acknowledge the Wajarri Yamatji people as the traditional owners of the Observatory site. Support for the operation of the MWA is provided by the Australian Government Department of Industry and Science and Department of Education (National Collaborative Research Infrastructure Strategy: NCRIS), under a contract to Curtin University administered by Astronomy Australia Limited. We acknowledge the iVEC Petabyte Data Store and the Initiative in Innovative Computing and the CUDA Center for Excellence sponsored by NVIDIA at Harvard University.

The *Fermi* LAT Collaboration acknowledges generous ongoing support from a number of agencies and institutes that have supported both the development and the operation of the LAT as well as scientific data analysis. These include the National Aeronautics and Space Administration and the Department of Energy in the United States, the Commissariat à l'Énergie Atomique and the Centre National de la Recherche Scientifique / Institut National de Physique Nucléaire et de Physique des Particules in France, the Agenzia Spaziale Italiana and the Istituto Nazionale di Fisica Nucleare in Italy, the Ministry of Education, Culture, Sports, Science and Technology (MEXT), High Energy Accelerator Research Organization (KEK) and Japan Aerospace Exploration Agency (JAXA) in Japan, and the K. A. Wallenberg Foundation, the Swedish Research Council and the Swedish National Space Board in Sweden. Additional support for science analysis during the operations phase is gratefully acknowledged from the Istituto Nazionale di Astrofisica in Italy and the Centre National d'Études Spatiales in France.

## References

- Abdo, A. A., Ackermann, M., Ajello, M., et al. 2010, *ApJS*, 188, 405  
 Acero, F., Ackermann, M., Ajello, M., et al. 2015, *ApJS*, 218, 23  
 Ackermann, M., Ajello, M., Allafort, A., et al. 2011a, *ApJ*, 741, 30  
 Ackermann, M., Ajello, M., Allafort, A., et al. 2011b, *ApJ*, 743, 171  
 Ackermann, M., Ajello, M., Atwood, W. B., et al. 2015, *ApJ*, 810, 14  
 Bock, D. C.-J., Large, M. I., & Sadler, E. M. 1999, *AJ*, 117, 1578  
 Chhetri, R., Ekers, R. D., Mahony, E. K., Jones, P. A., Massardi, M., Ricci, R., & Sadler, E. M. 2012, *MNRAS*, 422, 2274  
 Cohen, A. S., Lane, W. M., Cotton, W. D., Kassim, N. E., Lazio, T. J. W., Perley, R. A., Condon, J. J., & Erickson, W. C. 2007, *AJ*, 134, 1245  
 Condon, J. J., Cotton, W. D., Greisen, E. W., Yin, Q. F., Perley, R. A., Taylor, G. B., & Broderick, J. J. 1998, *AJ*, 115, 1693  
 Fossati, G., Maraschi, L., Celotti, A., Comastri, A., & Ghisellini, G. 1998, *MNRAS*, 299, 433



- Ghirlanda, G., Ghisellini, G., Tavecchio, F., & Foschini, L. 2010, *MNRAS*, 407, 791
- Ghirlanda, G., Ghisellini, G., Tavecchio, F., Foschini, L., & Bonnoli, G. 2011, *MNRAS*, 413, 852
- Giommi, P., & Padovani, P. 2015, *MNRAS*, 450, 2404
- Giroletti, M., Orienti, M., D’Ammando, F., et al. 2015, *aska.conf*, 153
- Herald, G. H., Pizzo, R. F., Orrú, E., et al. 2015, *A&A*, 582, A123
- Hurley-Walker, N., Morgan, J., Wayth, R. B., et al. 2014, *PASA*, 31, e045
- Komatsu, E., Dunkley, J., Nolta, M. R., et al. 2009, *ApJS*, 180, 330
- Mahony, E. K., Sadler, E. M., Murphy, T., Ekers, R. D., Edwards, P. G., & Mas-sardi, M. 2010, *ApJ*, 718, 587
- Massardi, M., Bonaldi, A., Bonavera, L., De Zotti, G., Lopez-Caniego, M., & Galluzzi, V. 2016, *MNRAS*, 455, 3249
- Massaro, E., Giommi, P., Leto, C., et al. 2009, *A&A*, 495, 691
- Massaro, F., D’Abrusco, R., Giroletti, M., Paggi, A., Masetti, N., Tosti, G., Nori, M., & Funk, S. 2013a, *ApJS*, 207, 4
- Massaro, F., Giroletti, M., Paggi, A., D’Abrusco, R., Tosti, G., & Funk, S. 2013b, *ApJS*, 208, 15
- Massaro, F., Giroletti, M., D’Abrusco, R., Masetti, N., Paggi, A., Cowperthwaite, P. S., Tosti, G., & Funk, S. 2014, *ApJS*, 213, 3
- Massaro, E., Maselli, A., Leto, C., Marchegiani, P., Perri, M., Giommi, P., & Piranomonte, S. 2015, *Ap&SS*, 357, 75
- Mauch, T., Murphy, T., Buttery, H. J., Curran, J., Hunstead, R. W., Piestrzynski, B., Robertson, J. G., & Sadler, E. M. 2003, *MNRAS*, 342, 1117
- Meyer, E. T., Fossati, G., Georganopoulos, M., & Lister, M. L. 2011, *ApJ*, 740, 98
- Murphy, T., Sadler, E. M., Ekers, R. D., et al. 2010, *MNRAS*, 402, 2403
- Nolan, P. L., Abdo, A. A., Ackermann, M., et al. 2012, *ApJS*, 199, 31
- Nori, M., Giroletti, M., Massaro, F., D’Abrusco, R., Paggi, A., Tosti, G., & Funk, S. 2014, *ApJS*, 212, 3
- Pavlidou, V., Richards, J. L., Max-Moerbeck, W., et al. 2012, *ApJ*, 751, 149
- Potter, W. J., & Cotter, G. 2013, *MNRAS*, 436, 304
- Taylor, M. B. 2005, *ASPC*, 347, 29
- Tingay, S. J., Goeke, R., Bowman, J. D., et al. 2013, *PASA*, 30, e007
- Trüstedt, J., Kadler, M., Brüggem, M., et al. 2014, *evn.conf*, 43
- Urry, C. M., & Padovani, P. 1995, *PASP*, 107, 803
- van Haarlem, M. P., Wise, M. W., Gunst, A. W., et al. 2013, *A&A*, 556, A2
- Wayth, R. B., Lenc, E., Bell, M. E., et al. 2015, *PASA*, 32, e025
- 
- <sup>1</sup> INAF Osservatorio di Radioastronomia, via Gobetti 101, 40129 Bologna, Italy
- <sup>2</sup> Physics Department, University of Turin, via Pietro Giuria 1, I-10125 Turin, Italy
- <sup>3</sup> Department of Physical Sciences, University of Naples Federico II, via Cinthia 9, 80126 Naples, Italy
- <sup>4</sup> Dipartimento di Fisica e Astronomia, Università di Bologna, via Ranzani 1, 40127, Bologna, Italy
- <sup>5</sup> Sydney Institute for Astronomy (SifA), School of Physics, The University of Sydney, NSW 2006, Australia
- <sup>6</sup> ARC Centre of Excellence for All-sky Astrophysics (CAASTRO)
- <sup>7</sup> International Centre for Radio Astronomy Research (ICRAR), Curtin University, Bentley, WA 6102, Australia
- <sup>8</sup> School of Chemical and Physical Sciences, Victoria University of Wellington, PO Box 600, Wellington 6140, New Zealand
- <sup>9</sup> University of Crete and Foundation for Research and Technology - Hellas, 71003, Heraklion, Greece
- <sup>10</sup> CSIRO Astronomy and Space Science (CASS), PO Box 76, Epping, NSW 1710, Australia
- <sup>11</sup> Department of Physics and Electronics, Rhodes University, PO Box 94, Grahamstown 6140, South Africa
- <sup>12</sup> School of Earth and Space Exploration, Arizona State University, Tempe, AZ 85287, USA
- <sup>13</sup> Research School of Astronomy and Astrophysics, Australian National University, Canberra, ACT 2611, Australia
- <sup>14</sup> MIT Haystack Observatory, Westford, MA 01886, USA
- <sup>15</sup> Raman Research Institute, Bangalore 560080, India
- <sup>16</sup> Kavli Institute for Astrophysics and Space Research, Massachusetts Institute of Technology, Cambridge, MA 02139, USA
- <sup>17</sup> Dunlap Institute for Astronomy and Astrophysics, University of Toronto, ON, M5S 3H4, Canada
- <sup>18</sup> Harvard-Smithsonian Center for Astrophysics, Cambridge, MA 02138, USA
- <sup>19</sup> Department of Physics, University of Washington, Seattle, WA 98195, USA
- <sup>20</sup> Department of Physics, University of Wisconsin–Milwaukee, Milwaukee, WI 53201, USA
- <sup>21</sup> Department of Atmospheric, Oceanic and Space Sciences, University of Michigan, Ann Arbor, MI 48109, USA
- <sup>22</sup> School of Physics, The University of Melbourne, Parkville, VIC 3010, Australia
- <sup>23</sup> National Centre for Radio Astrophysics, Tata Institute for Fundamental Research, Pune 411007, India
- <sup>24</sup> Netherlands Institute for Radio Astronomy (ASTRON), PO Box 2, 7990 AA Dwingeloo, The Netherlands
- <sup>25</sup> National Radio Astronomy Observatory, Charlottesville and Greenbank, USA
- <sup>26</sup> SKA Organisation, Macclesfield SK11 9DL, UK

Table 5. MWACS-BZCat sources

BZCat name	Class	$z$	$S_1$ (mJy)	MWACS name	$S_{0.18}$ (Jy)	$\sigma_{S_{0.18}}$ (Jy)	$\alpha_{\text{low}}$	$\sigma_{\alpha_{\text{low}}}$	Fit
5BZQ J0004–4736	fsrq	0.884	909	J0004.5–4736	0.47	0.06	0.16	0.39	0
5BZQ J0005–1648	fsrq	0.78	263	J0005.3–1648	0.58	0.08	1.29	0.40	0
5BZQ J0010–3027	fsrq	1.19	315	J0010.5–3027	0.45	0.06	1.42	0.34	0
5BZQ J0011–2612	fsrq	1.096	210	J0011.0–2612	0.26	0.04	–0.25	0.59	0
5BZQ J0015–1812	fsrq	0.743	387	J0015.0–1812	0.42	0.06	1.14	0.44	0
5BZQ J0017–2748	fsrq	1.169	344	J0018.0–2748	0.24	0.04	–0.50	1.02	0
5BZQ J0019–3031	fsrq	2.677	507	J0019.7–3031	0.30	0.05	–0.29	0.59	0
5BZQ J0025–2227	fsrq	0.834	202	J0025.4–2227	0.24	0.04	0.97	0.59	0
5BZQ J0030–4224	fsrq	0.495	425	J0030.3–4224	0.69	0.08	0.01	0.29	0
5BZQ J0032–2649	fsrq	1.47	135	J0032.5–2648	0.45	0.06	–0.42	0.29	1
5BZB J0032–2849	bll	0.324	160	J0032.5–2849	0.40	0.06	0.20	0.47	0
5BZQ J0038–2459	fsrq	0.498	413	J0038.2–2459	0.40	0.05	–0.43	0.49	0
5BZB J0040–2719	bll	0.172	160	J0040.2–2719	0.63	0.08	0.78	0.19	1
5BZQ J0049–5738	fsrq	1.797	2111	J0050.0–5738	3.41	0.37	0.77	0.18	0
5BZU J0058–5659	bcu	...	485	J0058.7–5658	0.37	0.06	0.96	0.50	0
5BZQ J0102–2646	fsrq	1.597	291	J0102.9–2646	0.41	0.05	–0.22	0.51	0
5BZQ J0115–2804	fsrq	2.579	439	J0115.4–2805	0.41	0.06	0.21	0.46	0
5BZQ J0117–3357	fsrq	0.647	415	J0117.7–3357	1.48	0.16	0.69	0.20	0
5BZQ J0118–2141	fsrq	1.165	447	J0118.9–2141	0.65	0.09	0.46	0.46	0
5BZB J0120–2701	bll	...	934	J0120.5–2701	1.80	0.19	0.46	0.19	0
5BZQ J0124–5113	fsrq	1.104	251	J0124.9–5113	0.40	0.06	0.73	0.47	0
5BZQ J0126–2222	fsrq	0.717	612	J0126.2–2222	2.67	0.29	0.53	0.18	0
5BZQ J0132–1654	fsrq	1.02	830	J0132.7–1655	1.30	0.15	–0.27	0.28	0
5BZU J0133–5200	bcu	...	352	J0133.1–5200	0.31	0.05	0.46	0.64	0
5BZQ J0134–3843	fsrq	2.14	569	J0134.5–3843	0.94	0.11	0.68	0.27	0
5BZQ J0135–2008	fsrq	1.141	559	J0135.6–2009	0.50	0.07	–0.34	0.44	0
5BZQ J0137–2430	fsrq	0.835	1181	J0137.6–2431	4.04	0.43	0.75	0.17	0
5BZQ J0138–2711	fsrq	2.999	261	J0138.1–2711	0.35	0.05	1.26	0.51	0
5BZQ J0138–2254	fsrq	1.895	512	J0138.9–2255	2.60	0.28	0.76	0.18	0
5BZQ J0145–2733	fsrq	1.148	923	J0145.0–2733	0.95	0.11	–0.06	0.31	0
5BZG J0146–5202	bll-g	0.098	324	J0146.8–5202	1.58	0.17	1.01	0.19	0
5BZQ J0153–3310	fsrq	0.61	1186	J0153.1–3310	0.64	0.08	–0.10	0.38	0
5BZQ J0154–5107	fsrq	1.582	447	J0154.3–5107	0.23	0.04	1.41	0.55	0
5BZQ J0204–1701	fsrq	1.74	1220	J0204.9–1701	1.15	0.14	0.08	0.31	0
5BZU J0210–5101	bcu	1.003	3493	J0210.7–5100	6.02	0.64	0.50	0.17	0
5BZQ J0222–1615	fsrq	0.698	590	J0222.0–1615	1.18	0.14	0.88	0.30	0
5BZQ J0222–3441	fsrq	1.49	683	J0222.9–3441	0.44	0.07	–0.63	0.61	0
5BZQ J0223–5347	fsrq	0.569	184	J0223.5–5347	0.26	0.04	1.08	0.51	0
5BZQ J0228–5546	fsrq	2.464	352	J0228.3–5545	0.34	0.06	0.92	0.77	0
5BZQ J0231–3935	fsrq	1.646	372	J0231.8–3935	0.41	0.06	0.00	0.53	0
5BZQ J0235–4737	fsrq	1.504	697	J0235.1–4737	0.77	0.09	0.60	0.25	0
5BZQ J0236–2953	fsrq	2.102	313	J0236.5–2953	0.34	0.05	0.51	0.62	0
5BZQ J0246–4651	fsrq	1.385	1498	J0246.0–4651	3.23	0.34	0.70	0.18	0
5BZB J0248–1631	bll	...	520	J0248.1–1631	1.71	0.19	0.65	0.21	0
5BZQ J0252–2219	fsrq	1.419	443	J0252.8–2219	0.94	0.11	0.35	0.27	0
5BZQ J0253–5441	fsrq	0.539	964	J0253.5–5441	0.84	0.10	0.55	0.31	0
5BZQ J0256–2137	fsrq	1.47	367	J0256.2–2137	1.09	0.12	0.21	0.25	0
5BZQ J0256–3315	fsrq	1.915	180	J0256.7–3315	0.37	0.06	0.91	0.62	0
5BZQ J0258–5052	fsrq	0.834	741	J0258.6–5051	1.40	0.15	0.71	0.21	0
5BZB J0303–2407	bll	0.266	700	J0303.4–2407	2.50	0.27	0.45	0.18	0
5BZQ J0307–4857	fsrq	0.796	194	J0307.6–4856	0.40	0.05	1.43	0.41	0
5BZQ J0317–2803	fsrq	1.166	496	J0317.5–2803	1.74	0.19	0.56	0.20	0
5BZQ J0321–3122	fsrq	1.785	322	J0321.5–3122	0.97	0.11	0.63	0.26	0
5BZQ J0327–2202	fsrq	2.22	641	J0328.0–2202	0.82	0.10	–0.04	0.31	0
5BZQ J0329–2357	fsrq	0.895	683	J0329.9–2357	2.53	0.27	0.89	0.18	0
5BZQ J0331–2524	fsrq	2.69	320	J0331.1–2524	0.66	0.08	0.95	0.27	0
5BZB J0334–4008	bll	...	1042	J0334.2–4008	0.44	0.07	–0.41	0.66	0
5BZQ J0336–3616	fsrq	1.537	501	J0336.9–3615	0.37	0.06	0.81	0.65	0
5BZB J0340–2119	bll	0.233	1075	J0340.6–2119	1.62	0.18	0.12	0.20	0
5BZQ J0343–2530	fsrq	1.419	503	J0343.3–2530	1.45	0.16	0.82	0.19	0

5BZQ J0348–2749	fsrq	0.991	840	J0348.6–2749	1.08	0.13	–1.01	0.32	0
5BZB J0357–4955	bll	0.643	215	J0357.0–4955	0.44	0.06	1.64	0.40	0
5BZB J0359–2615	bll	...	796	J0359.5–2615	2.40	0.26	0.10	0.19	0
5BZQ J0402–3147	fsrq	1.288	681	J0402.3–3147	0.37	0.05	–0.59	0.56	0
5BZQ J0403–2444	fsrq	0.598	167	J0403.7–2444	0.29	0.05	2.86	0.47	0
5BZQ J0403–3605	fsrq	1.417	1151	J0403.9–3605	1.48	0.16	–0.11	0.19	0
5BZU J0406–3826	bcu	1.285	861	J0407.0–3826	0.46	0.07	–0.50	0.62	0
5BZQ J0411–5149	fsrq	1.257	351	J0411.6–5148	0.37	0.05	1.50	0.46	0
5BZQ J0412–4604	fsrq	2.223	439	J0412.8–4604	0.23	0.04	0.48	0.87	0
5BZU J0416–2056	bcu	0.807	2779	J0416.0–2056	12.62	1.34	0.67	0.17	0
5BZQ J0416–1851	fsrq	1.536	1248	J0416.6–1851	0.45	0.08	–0.15	0.63	0
5BZQ J0424–3848	fsrq	2.346	537	J0424.5–3848	1.47	0.16	0.40	0.22	0
5BZQ J0424–3756	fsrq	0.782	474	J0424.7–3756	0.59	0.08	0.30	0.39	0
5BZB J0425–5331	bll	...	261	J0425.1–5331	0.40	0.06	1.00	0.53	0
5BZB J0428–3756	bll	1.11	753	J0428.6–3756	0.92	0.11	0.77	0.24	0
5BZQ J0429–4328	fsrq	1.423	462	J0429.4–4328	1.40	0.15	1.00	0.21	0
5BZQ J0432–5109	fsrq	0.557	737	J0432.3–5109	1.48	0.16	0.29	0.22	0
5BZQ J0434–4355	fsrq	2.649	474	J0434.0–4355	1.09	0.12	0.49	0.25	0
5BZQ J0437–2954	fsrq	1.328	1092	J0437.6–2954	6.17	0.66	0.73	0.17	0
5BZQ J0438–2012	fsrq	2.146	494	J0438.8–2012	1.37	0.15	0.40	0.22	0
5BZU J0439–3210	bcu	...	374	J0439.5–3210	1.33	0.15	0.60	0.22	0
5BZQ J0439–3017	fsrq	1.447	249	J0439.9–3017	0.32	0.05	1.55	0.47	0
5BZQ J0440–4333	fsrq	2.852	6362	J0440.3–4333	7.63	0.81	–0.05	0.17	0
5BZQ J0441–4313	fsrq	0.593	334	J0441.3–4313	0.51	0.07	1.24	0.37	0
5BZB J0441–2952	bll-c	...	576	J0441.3–2952	1.96	0.21	0.27	0.20	0
5BZQ J0448–3659	fsrq	0.561	408	J0448.2–3659	1.61	0.17	0.73	0.17	0
5BZB J0449–4350	bll	0.205	359	J0449.4–4350	0.99	0.11	0.49	0.24	0
5BZQ J0451–4653	fsrq	0.602	476	J0451.8–4652	0.19	0.03	–0.13	0.94	2
5BZQ J0453–2807	fsrq	2.564	2541	J0453.2–2807	2.63	0.29	–0.11	0.18	1
5BZQ J0455–4615	fsrq	0.858	2100	J0455.8–4615	7.23	0.77	0.70	0.17	0
5BZQ J0513–2159	fsrq	1.296	648	J0513.8–2159	0.52	0.07	0.12	0.40	0
5BZQ J0515–4556	fsrq	0.194	1471	J0515.7–4556	2.37	0.26	0.82	0.22	0
5BZQ J0516–1603	fsrq	1.278	911	J0516.2–1603	3.25	0.35	0.69	0.19	0
5BZQ J0521–1737	fsrq	0.347	459	J0521.3–1737	1.21	0.14	0.44	0.26	0
5BZU J0522–3627	bcu	0.05655	15620	J0522.9–3627	61.86	6.39	0.62	0.14	0
5BZQ J0525–4557	fsrq	1.479	2126	J0525.5–4557	3.85	0.41	0.91	0.18	0
5BZQ J0525–4318	fsrq	2.164	456	J0525.9–4317	1.05	0.12	1.20	0.26	0
5BZQ J0526–4830	fsrq	1.3	377	J0526.3–4830	0.54	0.07	0.60	0.43	0
5BZB J0533–4632	bll	0.332	246	J0533.7–4631	0.67	0.09	0.78	0.40	0
5BZQ J0534–3747	fsrq	1.668	736	J0534.3–3747	2.24	0.24	0.24	0.17	0
5BZQ J0536–3401	fsrq	0.684	652	J0536.4–3401	0.49	0.08	–1.05	0.71	0
5BZB J0538–4405	bll	0.892	3729	J0538.8–4405	3.50	0.37	–0.29	0.19	0
5BZU J0539–1550	bcu	0.947	599	J0539.5–1550	0.84	0.11	0.52	0.33	0
5BZQ J0539–2839	fsrq	3.104	862	J0539.9–2839	0.58	0.07	–0.66	0.43	0
5BZQ J0540–5418	fsrq	1.185	387	J0540.7–5418	0.69	0.09	0.81	0.39	0
5BZQ J0549–5246	fsrq	0.447	140	J0549.7–5245	0.35	0.06	0.48	0.61	0
5BZG J0550–3216	bll-g	0.069	345	J0550.6–3216	2.32	0.25	0.75	0.19	0
5BZQ J0559–4529	fsrq	0.687	384	J0559.2–4529	0.37	0.05	0.73	0.53	0
5BZQ J0600–3937	fsrq	1.661	461	J0600.5–3937	0.64	0.09	–0.41	0.54	0
5BZQ J0608–2220	fsrq	1.926	678	J0609.0–2220	0.82	0.10	0.83	0.30	0
5BZQ J0609–1542	fsrq	0.324	2742	J0609.7–1542	2.17	0.24	–1.14	0.28	0
5BZQ J0612–3138	fsrq	0.873	613	J0612.4–3138	2.93	0.31	0.81	0.18	0
5BZQ J0614–2536	fsrq	2.15	419	J0614.2–2537	0.65	0.08	–0.14	0.40	0
5BZU J0620–2515	bcu	1.9	1214	J0620.5–2515	3.67	0.39	0.71	0.18	0
5BZQ J0623–4413	fsrq	0.688	766	J0623.5–4413	1.40	0.15	0.58	0.21	0
5BZB J0629–1959	bll	...	677	J0629.4–1959	0.67	0.10	–0.10	0.55	0
5BZQ J0631–4154	fsrq	1.416	685	J0631.2–4154	1.14	0.13	0.40	0.26	0
5BZQ J0632–5404	fsrq	0.193	171	J0631.9–5405	1.46	0.17	1.27	0.29	0
5BZQ J0632–2614	fsrq	0.717	432	J0632.1–2614	1.55	0.17	0.59	0.21	0
5BZQ J0648–4347	fsrq	1.029	265	J0648.2–4346	1.13	0.13	1.40	0.24	0
5BZQ J0648–3044	fsrq	1.153	898	J0648.2–3044	1.25	0.14	0.39	0.24	0
5BZQ J0648–1744	fsrq	1.232	1046	J0648.4–1744	2.51	0.27	0.70	0.20	0
5BZQ J0659–2745	fsrq	1.727	541	J0659.8–2745	0.60	0.07	0.45	0.37	0
5BZQ J0726–4728	fsrq	1.686	490	J0726.4–4728	0.40	0.07	0.32	0.71	0

5BZQ J0728–4745	fsrq	2.282	376	J0728.3–4745	0.54	0.08	−0.46	0.62	0
5BZQ J0741–4709	fsrq	0.765	396	J0741.7–4709	0.29	0.05	0.27	0.89	0
5BZQ J2056–4714	fsrq	1.491	2138	J2056.2–4714	4.50	0.48	0.86	0.18	0
5BZU J2105–4848	bcu	1.041	1100	J2105.0–4848	3.43	0.37	0.85	0.18	0
5BZQ J2109–4110	fsrq	1.058	1823	J2109.5–4109	2.43	0.26	0.54	0.19	0
5BZQ J2126–4605	fsrq	1.67	1520	J2126.5–4605	2.84	0.30	0.83	0.18	0
5BZQ J2135–5006	fsrq	2.181	343	J2135.3–5006	0.17	0.03	3.02	0.62	0
5BZQ J2141–3729	fsrq	0.423	397	J2141.8–3728	0.85	0.10	0.44	0.36	0
5BZB J2143–3929	bll	0.429	143	J2143.0–3928	0.37	0.05	1.31	0.45	0
5BZQ J2148–1723	fsrq	2.13	805	J2148.6–1723	1.85	0.22	0.59	0.28	0
5BZQ J2150–2812	fsrq	0.865	307	J2150.8–2812	0.73	0.09	0.51	0.40	0
5BZQ J2151–2742	fsrq	1.485	315	J2151.3–2742	0.41	0.06	1.45	0.57	0
5BZQ J2151–3027	fsrq	2.345	1244	J2151.9–3027	0.82	0.10	1.50	0.46	0
5BZQ J2158–1501	fsrq	0.672	3021	J2158.0–1501	2.48	0.28	0.53	0.25	0
5BZB J2158–3013	bll	0.116	489	J2158.8–3013	0.82	0.10	0.92	0.33	0
5BZQ J2200–1632	fsrq	0.836	240	J2200.9–1632	0.93	0.12	0.52	0.44	0
5BZQ J2206–1835	fsrq	0.619	6399	J2206.1–1835	10.40	1.11	0.39	0.17	0
5BZQ J2207–5346	fsrq	1.215	1799	J2207.7–5346	2.91	0.31	0.74	0.18	0
5BZQ J2207–5707	fsrq	2.725	474	J2207.9–5707	0.66	0.09	0.45	0.39	0
5BZU J2209–2453	bcu	0.159	455	J2209.3–2453	3.87	0.41	0.79	0.18	0
5BZQ J2213–2529	fsrq	1.833	1210	J2213.0–2529	2.46	0.26	0.73	0.19	0
5BZQ J2219–2719	fsrq	3.634	304	J2219.5–2718	0.31	0.05	−0.29	0.79	2
5BZQ J2223–3455	fsrq	0.298	850	J2223.1–3455	2.86	0.31	0.52	0.18	0
5BZQ J2230–3942	fsrq	0.318	370	J2230.6–3942	1.09	0.13	1.04	0.26	0
5BZQ J2230–4416	fsrq	1.326	555	J2230.9–4416	0.51	0.06	0.96	0.30	0
5BZQ J2232–1659	fsrq	1.78	535	J2232.3–1658	0.72	0.10	−0.03	0.39	1
5BZQ J2239–5525	fsrq	1.975	296	J2239.1–5525	0.29	0.05	0.02	0.64	0
5BZB J2243–2544	bll	0.774	1102	J2243.4–2544	2.63	0.28	0.32	0.18	0
5BZQ J2246–5607	fsrq	1.325	510	J2246.3–5607	0.73	0.09	0.48	0.30	0
5BZQ J2247–3657	fsrq	2.252	1261	J2247.0–3657	4.68	0.48	0.67	0.14	0
5BZQ J2248–2702	fsrq	2.75	89	J2248.6–2703	0.57	0.07	1.45	0.27	0
5BZQ J2248–3235	fsrq	2.268	708	J2248.6–3235	0.39	0.05	−2.40	0.48	2
5BZQ J2249–3039	fsrq	1.307	432	J2249.3–3039	1.40	0.15	0.80	0.20	0
5BZU J2250–2806	bcu	0.525	306	J2250.7–2806	0.26	0.04	1.07	0.51	0
5BZU J2254–3209	bcu	0.189	655	J2254.5–3209	2.94	0.31	0.74	0.18	0
5BZQ J2254–4139	fsrq	1.765	435	J2254.6–4139	0.48	0.07	1.17	0.44	0
5BZQ J2256–2735	fsrq	1.751	425	J2255.9–2735	0.68	0.08	0.80	0.19	1
5BZQ J2258–2758	fsrq	0.926	1249	J2258.1–2758	1.36	0.15	0.58	0.20	0
5BZQ J2300–2644	fsrq	1.476	712	J2300.4–2644	2.12	0.23	0.64	0.18	0
5BZU J2303–1841	bcu	0.129	861	J2303.0–1841	4.91	0.52	0.82	0.17	0
5BZQ J2304–3625	fsrq	0.962	255	J2304.9–3625	0.82	0.09	1.03	0.24	0
5BZQ J2309–3059	fsrq	1.38	562	J2309.2–3058	0.37	0.05	−1.07	0.66	2
5BZG J2310–4347	bll-g	0.0887	153	J2310.7–4347	0.44	0.06	0.90	0.40	0
5BZQ J2314–3138	fsrq	1.323	825	J2314.8–3138	0.40	0.05	0.81	0.54	0
5BZQ J2316–4041	fsrq	2.448	511	J2316.8–4041	0.33	0.05	0.45	0.75	0
5BZQ J2324–3714	fsrq	0.37	385	J2324.1–3714	0.83	0.09	1.11	0.22	0
5BZQ J2327–1447	fsrq	2.465	719	J2327.7–1448	1.58	0.19	0.34	0.27	0
5BZQ J2329–4730	fsrq	1.302	3180	J2329.3–4730	2.79	0.30	−0.03	0.18	0
5BZQ J2329–4955	fsrq	0.518	558	J2329.3–4955	0.58	0.07	0.97	0.29	0
5BZQ J2330–4539	fsrq	0.447	1476	J2330.6–4539	1.80	0.19	−0.16	0.20	0
5BZQ J2331–1556	fsrq	1.153	1335	J2331.6–1557	2.31	0.25	0.55	0.20	0
5BZU J2333–2343	bcu	0.0477	782	J2333.9–2343	0.48	0.06	3.47	0.42	0
5BZQ J2336–4115	fsrq	1.406	531	J2336.5–4114	0.65	0.08	−1.76	0.61	2
5BZQ J2339–3310	fsrq	1.802	1284	J2339.9–3310	3.62	0.39	0.54	0.18	0
5BZQ J2343–2858	fsrq	1.936	112	J2343.3–2858	0.26	0.04	0.68	0.51	0
5BZQ J2348–1631	fsrq	0.576	2642	J2348.0–1631	2.79	0.30	0.33	0.19	0
5BZQ J2353–2743	fsrq	0.889	169	J2353.1–2743	0.54	0.07	0.32	0.32	0
5BZB J2353–3037	bll	0.737	397	J2353.8–3038	0.56	0.07	0.62	0.32	0
5BZU J2354–4106	bcu	0.632	620	J2354.1–4106	1.09	0.12	0.57	0.23	0
5BZQ J2354–1513	fsrq	2.675	865	J2354.5–1513	1.16	0.14	−0.49	0.34	0
5BZQ J2355–3357	fsrq	0.702	330	J2355.4–3358	0.98	0.11	1.29	0.24	0
5BZQ J2357–5311	fsrq	1.006	1411	J2357.9–5311	1.67	0.18	0.55	0.20	0

**Table 6.** MWACS-3LAC sources

3FGL name	Other name	$z$	Class	$S_{\gamma, E > 0.1 \text{ GeV}}$ ( $10^{-12} \text{ erg cm}^{-2} \text{ s}^{-1}$ )	$\sigma_{S_{\gamma}}$	$\Gamma$	$\sigma_{\Gamma}$	MWACS name	$S_{0.18}$ (Jy)	$\sigma_{S_{0.18}}$ (Jy)	$\alpha_{\text{low}}$	$\sigma_{\alpha_{\text{low}}}$
J0004.7–4740	PKS 0002–478	0.88	fsrq	9.2	0.8	2.40	0.08	J0004.5–4736	0.47	0.06	0.16	0.39
J0030.3–4223	PKS 0027–426	0.495	fsrq	19.8	0.9	2.58	0.04	J0030.3–4224	0.69	0.08	0.01	0.29
J0032.3–2852	PMN J0032–2849	0.324	bll	2.6	0.6	2.19	0.18	J0032.5–2849	0.40	0.06	0.20	0.47
J0038.0–2501	PKS 0035–252	1.196	fsrq	6.6	0.8	2.44	0.09	J0038.2–2459	0.40	0.05	–0.43	0.49
J0039.0–2218	PMN J0039–2220	0.06438	bcu	2.3	0.8	1.72	0.20	J0039.1–2220	0.31	0.05	2.76	0.49
J0049.4–5401	PMN J0049–5402	...	cand	3.1	0.7	2.14	0.16	J0049.8–5402	0.48	0.06	0.29	0.38
J0049.8–5737	PKS 0047–579	1.797	fsrq	6.1	0.8	2.46	0.11	J0050.0–5738	3.41	0.37	0.77	0.18
J0118.8–2142	PKS 0116–219	1.165	fsrq	28.5	1.8	2.35	0.05	J0118.9–2141	0.65	0.09	0.46	0.46
J0120.4–2700	PKS 0118–272	...	bll	42.4	2.2	1.91	0.03	J0120.5–2701	1.80	0.19	0.46	0.19
J0126.1–2227	PKS 0123–226	0.72	fsrq	8.3	1.0	2.43	0.09	J0126.2–2222	2.67	0.29	0.53	0.18
J0132.6–1655	PKS 0130–17	1.02	fsrq	26.2	1.1	2.43	0.04	J0132.7–1655	1.30	0.15	–0.27	0.28
J0133.2–5159	PKS 0131–522	...	bcu	3.3	0.7	2.63	0.19	J0133.1–5200	0.31	0.05	0.46	0.64
J0134.3–3842	PMN J0134–3843	2.14	fsrq	3.9	0.7	2.33	0.14	J0134.5–3843	0.94	0.11	0.68	0.27
J0137.6–2430	PKS 0135–247	0.835	fsrq	15.3	0.9	2.52	0.05	J0137.6–2431	4.04	0.43	0.75	0.17
J0145.1–2732	PKS 0142–278	1.148	fsrq	21.8	1.0	2.57	0.04	J0145.0–2733	0.95	0.11	–0.06	0.31
J0147.0–5204	PKS 0144–522	0.0981	bcu	4.0	0.7	2.20	0.13	J0146.8–5202	1.58	0.17	1.01	0.19
J0205.2–1700	PKS 0202–17	1.74	fsrq	18.2	0.9	2.76	0.05	J0204.9–1701	1.15	0.14	0.08	0.31
J0207.9–3846	PKS 0205–391	0.254	bcu	4.3	0.7	2.54	0.14	J0207.2–3857	0.95	0.11	0.44	0.24
J0210.7–5101	PKS 0208–512	1.003	bcu	51.1	1.5	2.17	0.03	J0210.7–5100	6.02	0.64	0.50	0.17
J0222.1–1616	PKS 0219–164	0.698	fsrq	8.5	0.9	2.60	0.09	J0222.0–1615	1.18	0.14	0.88	0.30
J0228.3–5545	PKS 0226–559	2.464	fsrq	12.2	0.8	2.43	0.06	J0228.3–5545	0.34	0.06	0.92	0.77
J0230.6–5757	PKS 0229–581	0.03199	bll	2.3	0.7	1.68	0.29	J0231.1–5754	0.38	0.07	1.73	0.60
J0245.9–4651	PKS 0244–470	1.385	fsrq	56.1	1.4	2.27	0.03	J0246.0–4651	3.23	0.34	0.70	0.18
J0252.8–2218	PKS 0250–225	1.427	fsrq	57.1	1.6	2.15	0.03	J0252.8–2219	0.94	0.11	0.35	0.27
J0253.1–5438	PKS 0252–549	0.539	fsrq	4.7	0.7	2.45	0.12	J0253.5–5441	0.84	0.10	0.55	0.31
J0303.4–2407	PKS 0301–243	0.26	bll	65.9	2.7	1.92	0.02	J0303.4–2407	2.50	0.27	0.45	0.18
J0305.2–1607	PKS 0302–16	...	cand	3.0	0.9	1.69	0.19	J0305.2–1608	4.95	0.53	0.87	0.18
J0326.0–1842	PMN J0325–1843	...	cand	2.9	0.8	2.21	0.23	J0325.9–1844	0.61	0.09	–1.87	0.52
J0334.3–4008	PKS 0332–403	1.357	bll	42.3	1.7	2.00	0.04	J0334.2–4008	0.44	0.07	–0.41	0.66
J0336.9–3622	PKS 0335–364	1.537	fsrq	3.6	0.8	2.44	0.14	J0336.9–3615	0.37	0.06	0.81	0.65
J0339.2–1738	PKS 0336–177	0.0655	bcu	6.8	1.1	1.93	0.10	J0339.2–1736	0.52	0.08	–0.17	0.61
J0340.5–2119	PKS 0338–214	0.223	bll	7.2	0.9	2.22	0.10	J0340.6–2119	1.62	0.18	0.12	0.20
J0343.2–2534	PKS 0341–256	1.419	fsrq	9.4	0.9	2.56	0.08	J0343.3–2530	1.45	0.16	0.82	0.19
J0348.6–2748	PKS 0346–27	0.991	fsrq	5.0	0.8	2.38	0.12	J0348.6–2749	1.08	0.13	–1.01	0.32
J0357.1–4957	PKS 0355–500	0.643	bll	4.3	0.7	2.10	0.13	J0357.0–4955	0.44	0.06	1.64	0.40
J0359.3–2612	PKS 0357–264	...	bll	2.9	0.8	2.19	0.18	J0359.5–2615	2.40	0.26	0.10	0.19
J0401.8–3144	PKS 0400–319	1.288	fsrq	3.6	0.7	2.54	0.20	J0402.3–3147	0.37	0.05	–0.59	0.56
J0403.7–2442	TXS 0401–248	0.598	fsrq	2.9	0.7	2.37	0.18	J0403.7–2444	0.29	0.05	2.86	0.47
J0403.9–3604	PKS 0402–362	1.417	fsrq	85.3	1.5	2.27	0.03	J0403.9–3605	1.48	0.16	–0.11	0.19
J0407.1–3825	PKS 0405–385	1.285	fsrq	21.7	1.1	2.40	0.04	J0407.0–3826	0.46	0.07	–0.50	0.62
J0416.6–1850	PKS 0414–189	1.421	fsrq	14.0	1.0	2.34	0.06	J0416.6–1851	0.45	0.08	–0.15	0.63
J0425.0–5331	PMN J0425–5331	0.39	bll	9.3	0.8	2.34	0.08	J0425.1–5331	0.40	0.06	1.00	0.53
J0428.6–3756	PKS 0426–380	1.105	bll	184.0	4.2	1.95	0.02	J0428.6–3756	0.92	0.11	0.77	0.24
J0449.4–4350	PKS 0447–439	0.205	bll	123.1	3.8	1.85	0.02	J0449.4–4350	0.99	0.11	0.49	0.24
J0453.2–2808	PKS 0451–28	2.564	fsrq	25.0	1.0	2.63	0.04	J0453.2–2807	2.63	0.29	–0.11	0.18
J0455.7–4617	PKS 0454–46	0.858	fsrq	22.8	1.0	2.55	0.04	J0455.8–4615	7.23	0.77	0.70	0.17
J0505.5–1558	TXS 0503–160	...	cand	4.1	0.8	2.10	0.14	J0505.6–1558	1.94	0.22	0.53	0.23
J0521.4–1740	TXS 0519–176	0.347	fsrq	6.4	0.9	2.43	0.11	J0521.3–1737	1.21	0.14	0.44	0.26
J0522.9–3628	PKS 0521–36	0.0553	bcu	61.8	1.6	2.34	0.03	J0522.9–3627	61.86	6.39	0.62	0.14
J0525.3–4558	PKS 0524–460	1.479	fsrq	3.6	0.8	2.20	0.16	J0525.5–4557	3.85	0.41	0.91	0.18
J0525.8–2014	PMN J0525–2010	...	cand	3.6	0.8	2.06	0.16	J0525.4–2011	1.14	0.14	0.95	0.30
J0526.2–4829	PKS 0524–485	1.299	fsrq	17.1	1.3	2.29	0.06	J0526.3–4830	0.54	0.07	0.60	0.43
J0538.8–4405	PKS 0537–441	0.892	bll	308.3	4.9	1.93	0.01	J0538.8–4405	3.50	0.37	–0.29	0.19
J0540.0–2837	PKS 0537–286	3.104	fsrq	17.3	1.1	2.78	0.06	J0539.9–2839	0.58	0.07	–0.66	0.43
J0540.5–5416	PKS 0539–543	1.185	fsrq	12.0	0.9	2.63	0.07	J0540.7–5418	0.69	0.09	0.81	0.39
J0550.6–3217	PKS 0548–322	0.069	bll	4.0	1.0	1.61	0.16	J0550.6–3216	2.32	0.25	0.75	0.19
J0600.9–3943	PKS 0558–396	1.661	fsrq	6.6	1.2	2.81	0.13	J0600.5–3937	0.64	0.09	–0.41	0.54
J0629.4–1959	PKS 0627–199	1.724	bll	38.2	1.8	2.18	0.03	J0629.4–1959	0.67	0.10	–0.10	0.55
J0648.1–3045	PKS 0646–306	1.153	fsrq	15.7	1.2	2.56	0.07	J0648.2–3044	1.25	0.14	0.39	0.24
J0706.1–4849	PMN J0705–4847	...	cand	9.0	1.2	2.41	0.09	J0705.9–4847	0.33	0.05	1.17	0.55
J0726.6–4727	PMN J0726–4728	1.686	fsrq	17.4	1.4	2.46	0.06	J0726.4–4728	0.40	0.07	0.32	0.71
J0732.2–4638	PKS 0731–465	...	cand	9.3	1.2	2.35	0.17	J0732.7–4640	2.08	0.23	0.21	0.21
J2051.8–5535	PMN J2052–5533	...	cand	6.0	1.0	2.58	0.15	J2052.2–5532	0.71	0.11	0.65	0.53
J2056.2–4714	PKS 2052–47	1.491	fsrq	77.4	1.8	2.26	0.03	J2056.2–4714	4.50	0.48	0.86	0.18
J2126.5–4605	PKS 2123–463	1.67	fsrq	28.7	1.1	2.50	0.04	J2126.5–4605	2.84	0.30	0.83	0.18
J2135.3–5008	PMN J2135–5006	2.181	fsrq	12.0	1.2	2.47	0.07	J2135.3–5006	0.17	0.03	3.02	0.62

J2141.7–3734	PKS 2138–377	0.423	fsrq	6.7	0.9	2.59	0.11	J2141.8–3728	0.85	0.10	0.44	0.36
J2143.1–3928	PMN J2143–3929	0.429	bll	5.7	0.9	2.07	0.13	J2143.0–3928	0.37	0.05	1.31	0.45
J2151.6–2744	PMN J2151–2742	1.485	fsrq	4.4	0.8	2.51	0.15	J2151.3–2742	0.41	0.06	1.45	0.57
J2151.8–3025	PKS 2149–306	2.345	fsrq	29.6	1.3	2.61	0.08	J2151.9–3027	0.82	0.10	1.50	0.46
J2158.0–1501	PKS 2155–152	0.672	fsrq	12.6	1.1	2.27	0.07	J2158.0–1501	2.48	0.28	0.53	0.25
J2158.8–3013	PKS 2155–304	0.116	bll	230.5	6.2	1.75	0.02	J2158.8–3013	0.82	0.10	0.92	0.33
J2207.8–5345	PKS 2204–54	1.215	fsrq	12.9	0.8	2.58	0.06	J2207.7–5346	2.91	0.31	0.74	0.18
J2213.1–2532	PKS 2210–25	1.833	fsrq	7.6	0.8	2.55	0.10	J2213.0–2529	2.46	0.26	0.73	0.19
J2222.3–3500	PKS 2220–351	0.298	fsrq	3.1	0.6	2.37	0.18	J2223.1–3455	2.86	0.31	0.52	0.18
J2230.6–4419	PKS 2227–445	1.326	fsrq	3.7	0.7	2.57	0.17	J2230.9–4416	0.51	0.06	0.96	0.30
J2243.4–2541	PKS 2240–260	0.774	bll	19.6	1.1	2.27	0.05	J2243.4–2544	2.63	0.28	0.32	0.18
J2248.6–3235	PKS 2245–328	2.268	fsrq	5.0	0.7	2.82	0.14	J2248.6–3235	0.39	0.05	-2.40	0.48
J2250.7–2806	PMN J2250–2806	0.525	bcu	47.1	1.7	2.18	0.03	J2250.7–2806	0.26	0.04	1.07	0.51
J2258.0–2759	PKS 2255–282	0.926	fsrq	48.7	1.5	2.17	0.04	J2258.1–2758	1.36	0.15	0.58	0.20
J2329.3–4955	PKS 2326–502	0.518	fsrq	147.6	2.3	2.12	0.02	J2329.3–4955	0.58	0.07	0.97	0.29
J2329.9–4734	PKS 2326–477	1.302	fsrq	4.3	0.9	2.23	0.16	J2329.3–4730	2.79	0.30	-0.03	0.18
J2336.5–4116	PKS 2333–415	1.406	fsrq	11.3	1.0	2.24	0.07	J2336.5–4114	0.65	0.08	-1.76	0.61
J2348.0–1630	PKS 2345–16	0.576	fsrq	29.4	1.7	2.20	0.05	J2348.0–1631	2.79	0.30	0.33	0.19
J2353.6–3037	PKS 2351–309	0.737	bll	5.3	0.9	2.28	0.13	J2353.8–3038	0.56	0.07	0.62	0.32
J2357.8–5310	PKS 2355–534	1.006	fsrq	11.8	1.2	2.46	0.07	J2357.9–5311	1.67	0.18	0.55	0.20
J2359.5–2052	TXS 2356–210	0.096	bll	3.8	0.7	2.02	0.16	J2359.3–2048	1.37	0.15	0.53	0.21

**Table 7.** UGS with MWACS sources in the 95% error ellipse

3FGL name	$S_{\gamma, E > 0.1 \text{ GeV}}$ ( $10^{-12} \text{ erg cm}^{-2} \text{ s}^{-1}$ )	$\sigma_{S_{\gamma}}$	$\Gamma$	$\sigma_{\Gamma}$	MWACS name	$S_{0.18}$ (Jy)	$\sigma_{S_{0.18}}$ (Jy)	$\alpha_{\text{low}}$	$\sigma_{\alpha_{\text{low}}}$
3FGL J0026.2–4812	3.58	0.68	2.19	0.15	J0025.6–4816	0.65	0.08	0.18	0.30
3FGL J0031.2–2320	2.66	0.66	2.14	0.17	J0030.6–2323	0.26	0.04	−0.26	0.80
3FGL J0121.8–3917	2.43	0.69	1.80	0.20	J0122.1–3919	0.32	0.05	0.50	0.43
3FGL J0133.2–4737	3.08	0.68	2.71	0.20	J0132.2–4742	0.32	0.05	−0.97	0.74
3FGL J0226.7–4747	4.60	0.75	2.92	0.19	J0226.0–4744	0.80	0.09	1.40	0.22
					J0226.3–4750	0.18	0.03	1.40	0.22
3FGL J0308.4–2852	2.98	0.72	2.54	0.25	J0308.2–2852	1.25	0.14	0.84	0.21
3FGL J0608.2–2306	3.27	0.78	2.20	0.16	J0607.5–2308	0.34	0.06	1.04	0.65
3FGL J0714.7–3924	5.64	1.26	2.38	0.14	J0714.1–3923	0.36	0.05	0.90	0.55
3FGL J0718.9–5004	5.07	1.00	2.39	0.14	J0719.2–5015	0.37	0.05	0.31	0.51
					J0719.3–4955	0.43	0.06	1.01	0.41
3FGL J2130.4–4237	8.01	0.97	2.56	0.10	J2130.2–4243	0.64	0.08	0.69	0.36
					J2131.1–4234	1.04	0.12	0.54	0.25